IOP Publishing Journal of Physics: Condensed Matter
J. Phys.: Condens. Matter **32** (2020) 205902 (8pp) https://doi.org/10.1088/1361-648X/ab6e8e

Band unfolding made simple

Sara G Mayo, Felix Yndurain and Jose M Soler

Departamento e Instituto de Física de la Materia Condensada (IFIMAC), Universidad Autónoma de Madrid, Cantoblanco, 28049 Madrid, Spain

E-mail: sara.garciamayo@uam.es

Received 14 October 2019, revised 3 January 2020
Accepted for publication 22 January 2020
Published 20 February 2020

Abstract

We present a simple view on band unfolding of the energy bands obtained from supercell calculations. It relies on the relationship between the local density of states in reciprocal space and the *fully unfolded* band structure. This provides an intuitive and valid approach not only for periodic, but also for systems with no translational symmetry. By *refolding* into the primitive Brillouin zone of the pristine crystal we recover the conventional unfolded bands. We implement our algorithm in the SIESTA package. As an application, we study a set of benchmark examples, ranging from simple defects on crystals to systems with increasing complexity and of current interest, as the effect of external pressure on rotated graphene bilayers.

Keywords: band unfolding, electronic structure, supercell, rotated graphene bilayers

(Some figures may appear in colour only in the online journal)

Introduction

Plots of so called energy bands are the most basic and used tool in interpreting the calculated electronic structure of simple crystals. Such plots represent the energy of the Bloch orbitals as a function of their crystal momentum in the primitive Brillouin zone (PBZ), that is, $E(\mathbf{k})$. These theoretical bands can be obtained within the tight-binding approximation, the density functional theory (DFT) or other electronic structure methods, and they are directly connected to results of angle resolved photoemission spectroscopy (ARPES) experiments. However, the simplicity of this approach disappears when the calculations involve large supercells with many atoms. As the size of the cell in real space increases, the first Brillouin zone in reciprocal space shrinks and more lines populate the band structure, hindering the extraction of useful information and the comparison with experiments.

Several authors have already explored the unfolding problem and developed specific techniques to unfold the supercell Brillouin zone into the PBZ. Some of the existing works focus on algorithms within the tight-binding approximation [1–4] or first principles calculations, employing as basis sets linear combinations of atomic orbitals [5], plane waves [6] or Wannier functions [7]. Another methodology studies the electronic structures of alloy systems [8, 9]. Other authors have delved into the theory of the problem and they have developed general reformulations of it [10–14].

Most of these methods focus on obtaining a direct relationship between the Brillouin zones of the primitive crystal cell and of the simulation supercell, by expanding the supercell states in a basis set with the periodicity of the crystal. In contrast, we aim to simplify the procedure and provide a link between existing methods by dividing the problem in two steps. First, we consider the *fully unfolded bands*, extended to the whole reciprocal space, through a Fourier decomposition of the Bloch wave functions of the system [14]. This yields a non-periodic description, interesting by itself. Second, by what we call *refolding* into the crystal PBZ, we recover the result that other authors refer to as unfolded bands.

Method

The basic steps of our unfolding method are schematically summarized in figure 1. We start by considering the energy bands not just as dispersion relations, but as the density of states in the (first) simulation Brillouin zone (SBZ), the reciprocal of the real-space simulation (super) cell (SC):

$$n_{\mathrm{SBZ}}(\mathbf{K},\epsilon) = \sum_i \delta(\epsilon - \epsilon_{\mathbf{K},i}) \tag{1}$$

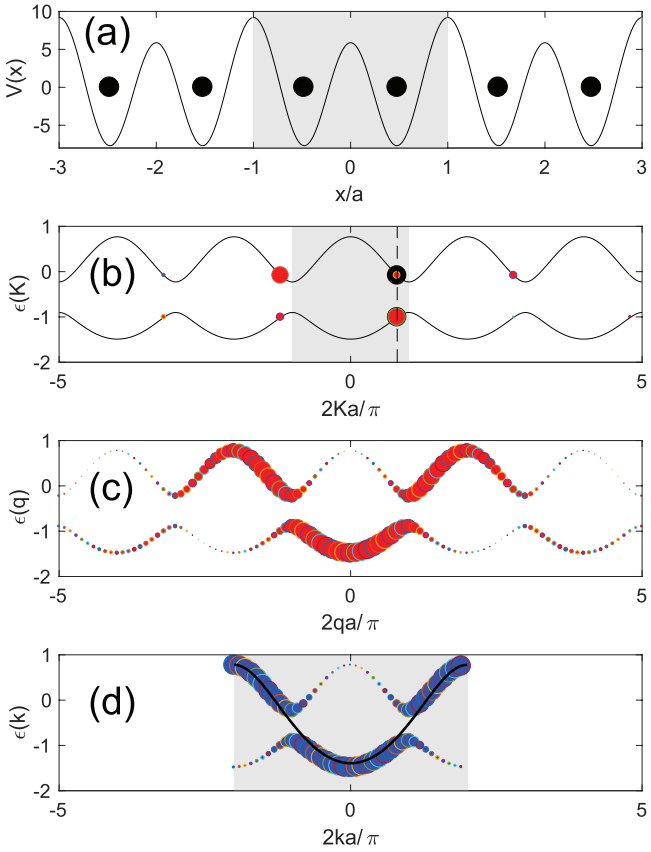

Figure 1. Scheme of the unfolding method. (a) 1D model of a chain of pseudo-atoms (dots) with an attractive gaussian potential (line). The atoms are paired, with a Peierls distortion of 2% relative to their undistorted distance a. The energy origin is the average potential and its units are $\hbar^2/(a^2 m_e)$. The unit cell of the distorted chain is shaded. (b) First two bands of the distorted chain, with its PBZ shaded. A random K point is singled out (dashed line). The (normalized) weights of the Bloch states at this K (black dots), are split according to the squared Fourier coefficients of their respective wave functions (red dots), appearing at $q = K + G$. Dot areas are proportional to weights. (c) Fully unfolded bands, obtained through the procedure described in (b) for all Ks in the PBZ. The non-periodic unfolded weights are the local DOS in Fourier space (qLDOS) $n(q, \epsilon)$. (d) Bands refolded into the PBZ of the undistorted chain (shaded region). The weight at each k (blue dots) is the sum over g of the unfolded weights in (c), at points $q = k + g$. The continuous line is the first band of the undistorted chain.

where $\mathbf{K}$ is a wave vector in the SBZ, and $\epsilon_{\mathbf{K},i}$ is the eigenvalue of its ith Bloch state, that is, band energy[1].

The normalization of $n_{\mathrm{SBZ}}(\mathbf{K}, \epsilon)$, as well as those of other densities defined below, is such that they are densities of states *per unit of macroscopic volume* (as well as per unit of their respective independent variables), what facilitates the comparison between simulation cells of different volumes.

Next, we split the normalized weight $\delta(\epsilon - \epsilon_{\mathbf{K},i})$ according to the squared Fourier coefficients of the corresponding wave function. Summing over Bloch states, we construct the *fully unfolded bands* as the spectral density, which can also be considered as the local density of states in reciprocal space (qLDOS):

$$n(\mathbf{q}, \epsilon) = \sum_i \int_{\mathrm{SBZ}} \mathrm{d}\mathbf{K}\, |\tilde{\psi}_{\mathbf{K},i}(\mathbf{q})|^2\, \delta(\epsilon - \epsilon_{\mathbf{K},i}) \tag{2}$$

where $\tilde{\psi}_{\mathbf{K},i}(\mathbf{q})$ is the Fourier transform of a Bloch wave function (normalized in the SC), $\psi_{\mathbf{K},i}(\mathbf{r}) = u_{\mathbf{K},i}(\mathbf{r})\mathrm{e}^{\mathrm{i}\mathbf{K}\mathbf{r}}$:

$$\psi_{\mathbf{K},i}(\mathbf{r}) = \frac{1}{(2\pi)^{3/2}} \int_{\infty} \mathrm{d}\mathbf{q}\, \tilde{\psi}_{\mathbf{K},i}(\mathbf{q})\, \mathrm{e}^{\mathrm{i}\mathbf{q}\mathbf{r}}, \tag{3}$$

$$\tilde{\psi}_{\mathbf{K},i}(\mathbf{q}) = (2\pi)^{3/2} \sum_{\mathbf{G}} \delta(\mathbf{K} + \mathbf{G} - \mathbf{q})\, \tilde{u}_{\mathbf{K},i,\mathbf{G}}, \tag{4}$$

$$\tilde{u}_{\mathbf{K},i,\mathbf{G}} = \frac{1}{V_{\mathrm{SC}}} \int_{\mathrm{SC}} \mathrm{d}\mathbf{r}\, u_{\mathbf{K},i}(\mathbf{r})\, \mathrm{e}^{-\mathrm{i}\mathbf{G}\mathbf{r}}, \tag{5}$$

with V_{SC} the volume of the SC and $\mathbf{G}$ its reciprocal wave vectors. Then, we can write $n(\mathbf{q}, \epsilon)$ as

$$n(\mathbf{q}, \epsilon) = \sum_i |\tilde{u}_{\mathbf{K_q},i,\mathbf{G_q}}|^2\, \delta(\epsilon - \epsilon_{\mathbf{K_q},i}), \tag{6}$$

where $\mathbf{K_q}$ and $\mathbf{G_q}$ are the unique vectors such that: $\mathbf{K_q}$ is within the SBZ; $\mathbf{G_q}$ is a reciprocal wave vector; and $\mathbf{K_q} + \mathbf{G_q} = \mathbf{q}$. A state $\psi_{\mathbf{K},i}$ will contribute to $n(\mathbf{q}, \epsilon)$ at points $\mathbf{q} = \mathbf{K} + \mathbf{G}$ for all $\mathbf{G} = \pi N/a$ vectors, due to Bloch's theorem. We emphasize that $\mathbf{q}$ extends to infinity and $n(\mathbf{q}, \epsilon)$ is not periodic in $\mathbf{q}$: although the energies at which $n(\mathbf{q}, \epsilon)$ can be nonzero are periodic, these 'bands' have a different weight at each Brillouin zone (figure 1(c)).

As can be seen by comparing with equation (2), the qLDOS is the Fourier-space equivalent of the real-space local density of states (rLDOS),

$$n(\mathbf{r}, \epsilon) = \frac{V_{\mathrm{SC}}}{(2\pi)^3} \sum_i \int_{\mathrm{SBZ}} \mathrm{d}\mathbf{K}\, |\psi_{\mathbf{K},i}(\mathbf{r})|^2\, \delta(\epsilon - \epsilon_{\mathbf{K},i}). \tag{7}$$

The total density of states (DOS) can be obtained by integration of either $n(\mathbf{r}, \epsilon)$ or $n(\mathbf{q}, \epsilon)$:

$$n(\epsilon) = \frac{1}{V_{\mathrm{SC}}} \int_{\mathrm{SC}} \mathrm{d}\mathbf{r}\, n(\mathbf{r}, \epsilon) = \frac{1}{(2\pi)^3} \int_{\infty} \mathrm{d}\mathbf{q}\, n(\mathbf{q}, \epsilon). \tag{8}$$

Since $|\tilde{\psi}_{\mathbf{K},i}(\mathbf{q})|^2$ is the probability of measuring momentum $\mathbf{q}$ of a given electron, $n(\mathbf{q}, \epsilon)$ is the probability of finding an electron (or an empty state) in the system with energy ϵ and momentum $\mathbf{q}$, and it can thus be directly related with ARPES results if matrix element effects are taken into account [14, 15, 16].

The qLDOS, that we call *fully unfolded bands*, is the same as the *spectral weight* of other authors [10, 12, 13] and the *plane-wave unfolded spectra* introduced by Kosugi *et al* [14]. Therefore, our approach is a different description, rather than a new method that yields different results. Our emphasis is to provide a clear and simple link with previous methods through the (L)DOS, as well as to generalise band structure analysis to non periodic systems.

The last step in our method is to *refold* $n(\mathbf{q}, \epsilon)$ into a *refolding Brillouin zone* (RBZ) as

$$n_{\mathrm{RBZ}}(\mathbf{k}, \epsilon) = \sum_{\mathbf{g}} n(\mathbf{k} + \mathbf{g}, \epsilon), \tag{9}$$

[1] Following conventional practice, we write the Bloch wave vector $\mathbf{K}$ as a subscript, even though it is a continuous variable.

where $\mathbf{k}$ is within the RBZ and $\mathbf{g} = \pi n/a$ are its reciprocal lattice vectors. Notice that, since $\sum_{\mathbf{G}} |\tilde{u}_{\mathbf{K},i,\mathbf{G}}|^2 = 1$, then $\sum_{\mathbf{G}} n(\mathbf{K}+\mathbf{G},\epsilon) = n_{\mathrm{SBZ}}(\mathbf{K},\epsilon)$, that is, refolding $n(\mathbf{q},\epsilon)$ back into the SBZ recovers the original bands.

Frequently, the simulation cell will be a supercell of the refolding cell. In these cases, the RBZ will be a supercell of the SBZ, and vectors $\mathbf{g}$ will belong to the set of $\mathbf{G}$s (figure 1(d)). Nevertheless, this condition is not necessary in our method, and in fact it will not be true in many cases, as for simulation cells of liquids or amorphous systems, or of defects that induce strong deformations[2].

The above full unfolding/refolding method can be immediately applied in a plane wave DFT code, since the Fourier coefficients of the Bloch wave functions are then directly available. The slow decay with momentum of all-electron wavefunctions can be addressed by using pseudopotentials or by introducing a momentum cutoff. For a basis of atomic orbitals, we expand the Bloch states as

$$\psi_{\mathbf{K},i}(\mathbf{r}) = \sum_{\mathbf{R}} \sum_{\mu} c_{\mathbf{K},i,\mu}\, \phi_{\mu}(\mathbf{r} - \mathbf{R} - \mathbf{r}_{\mu})\, \mathrm{e}^{\mathrm{i}\mathbf{K}(\mathbf{R}+\mathbf{r}_{\mu})}, \quad (10)$$

where $c_{\mathbf{K},i,\mu}$ are expansion coefficients and ϕ_{μ} are atomic orbitals centered at position $\mathbf{R}+\mathbf{r}_{\mu}$ ($\mathbf{R}$ being SC lattice vectors). Substituting into equation (5) we find

$$\tilde{u}_{\mathbf{K},i,\mathbf{G}} = \frac{(2\pi)^{3/2}}{V_{\mathrm{SC}}} \sum_{\mu} c_{\mathbf{K},i,\mu}\, \tilde{\phi}_{\mu}(\mathbf{K}+\mathbf{G})\, \mathrm{e}^{-\mathrm{i}\mathbf{G}\mathbf{r}_{\mu}}, \quad (11)$$

where $\tilde{\phi}_{\mu}(\mathbf{q})$ is the Fourier transform of the numerical atomic orbital $\phi_{\mu}(\mathbf{r})$, with well defined angular momentum quantum numbers (l_{μ}, m_{μ}), that can be decomposed into radial and angular parts:

$$\phi_{\mu}(\mathbf{r}) = \phi_{\mu}(r)\, Y_{l_{\mu},m_{\mu}}(\hat{\mathbf{r}}) \quad (12)$$

$$\tilde{\phi}_{\mu}(\mathbf{q}) = \tilde{\phi}_{\mu}(q)\, Y_{l_{\mu},m_{\mu}}(\hat{\mathbf{q}}) \quad (13)$$

$$\tilde{\phi}_{\mu}(q) = \sqrt{\frac{2}{\pi}}(-1)^{l_{\mu}} \int_0^{\infty} r^2 dr\, j_{l_{\mu}}(qr)\, \phi_{\mu}(r), \quad (14)$$

with $Y_{l,m}(\hat{\mathbf{r}})$ spherical harmonics and $j_l(x)$ spherical Bessel functions.

We have implemented this algorithm in the SIESTA package [17]. After a converged DFT SIESTA calculation, the hamiltonian and overlap matrices, in the atomic basis set, are calculated and written in a file. This file, as well as those specifying the radial numerical atomic orbitals, are read by an external utility program that calculates the fully unfolded and refolded spectra at the desired $\mathbf{q}$ and $\mathbf{k}$ band lines. Some SIESTA subroutines are also used by the unfolding/refolding program to obtain the wave function coefficients at each required $\mathbf{K}$ point of the SBZ, as well as to perform the Fourier transforms in equation (14).

[2] In these cases, however, the vector $\mathbf{K}$ such that $\mathbf{K}+\mathbf{G} = \mathbf{k}+\mathbf{g}$, will depend not only on $\mathbf{k}$ but also on $\mathbf{g}$. This will make the calculation of $n_{\mathrm{RBZ}}(\mathbf{k},\epsilon)$, at given $\mathbf{k}$ points, considerably more expensive.

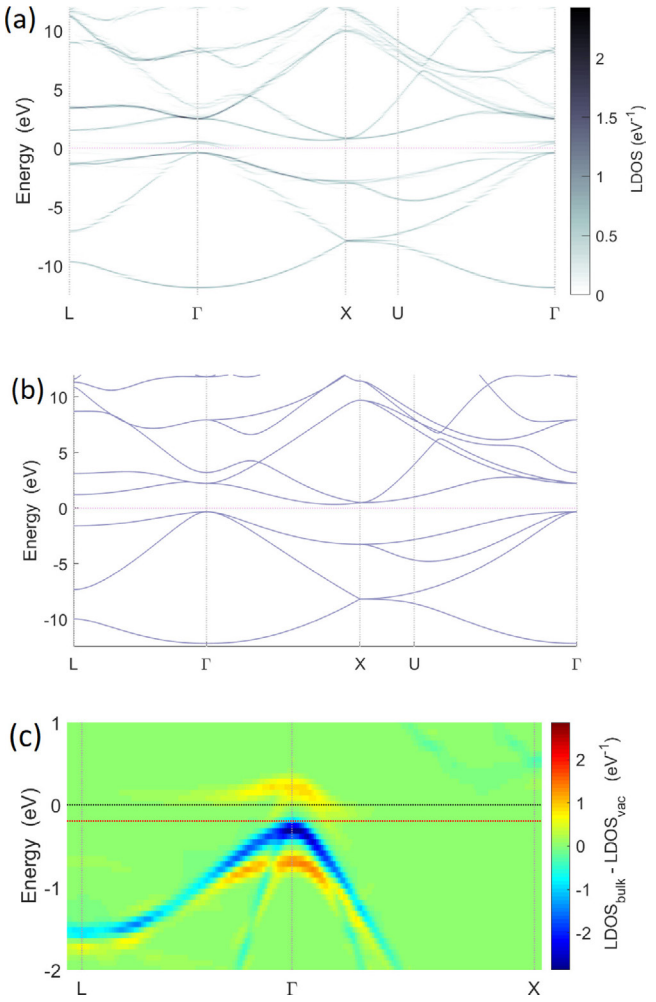

Figure 2. (a) Refolded bands, into the crystal PBZ, of a single vacancy in bulk Si. The darkness is proportional to the LDOS. Energies are relative to the Fermi level, set at zero (horizontal dotted line). Vertical dotted lines mark high symmetry points of the PBZ; (b) (conventional) bands of Si FCC crystal; (c) difference between the refolded LDOS of the defective Si and the pristine crystal, zoomed in the gap region, near the Γ point. States arising (vanishing) due to the vacancy appear in hot (cold) colours. The black (red) dashed line is the Fermi level of the perfect (defective) system.

Applications

We apply our previously described SIESTA implementation to a Si FCC crystal with a single vacancy, a model of amorphous Si (a-Si), a monolayer of graphene with a (585) divacancy, and a rotated graphene bilayer under pressure. We employed the GGA-PBE [18] functional for exchange and correlation and double-ζ + polarization (DZP) basis sets (double-ζ (DZ) for a-Si).

Vacancy in Si crystal

We model a vacancy in a Si FCC crystal using a 63-atom supercell. Its refolded bands into the crystal PBZ vectors are depicted in figure 2(a), and can be compared with the bands of the periodic crystal, in figure 2(b). Changes are appreciated at a careful sight. The refolded bands become blurred and

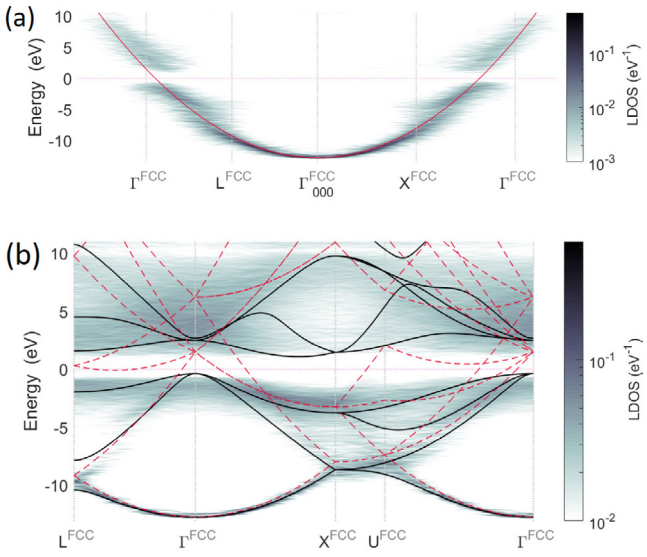

Figure 3. (a) Fully unfolded bands of a 512-atom cubic cell of amorphous silicon, along the (111) and (1 0 0) directions. Vertical lines indicate high symmetry points of the first and second Brillouin zones of the crystal. They are shown for reference but they are not special in the a-Si simulation cell. The red line is a fit to a free-electron dispersion relation with an effective mass $m^* = 1.1$; (b) refolding of the a-Si bands into the PBZ of crystalline silicon. Solid lines are the crystal bands. The refolded free-electron dispersion relation is shown with dashed lines.

widened due to the appearance of small splittings. Some of these are a consequence of the supercell approach and they become smoother in a larger SC.

The most relevant changes occur around the Fermi level. A new state arises within the gap, with higher weight around the Γ point. The top of the valence band, around Γ, decreases in energy and in weight. We show the difference between the crystal and defective refolded spectra in figure 2(d) around Γ, at the gap, to remark these changes.

Amorphous Si

A clear example of disorder is an amorphous solid. In this case, we cannot talk about a proper band structure, but yet the energy dispersion of the electron states provides interesting results. We studied the fully unfolded and refolded bands of a-Si using supercells of 216, 512 and 1024 atoms, modelled by Igram *et al* [19], obtaining equivalent results for all cases. We present the results for the 512-atom supercell.

In figure 3(a) we show those corresponding to the $L-\Gamma$ and $\Gamma-X$ directions of the FCC crystal, up to the second Brillouin zone. As expected from the isotropic character of the amorphous solid, its unfolded bands are essentially identical in all directions, with a radial symmetry, yielding a widened free-electron dispersion with an effective mass $m^* = 1.1$ and a gap of 1.5 eV, consistent with existing values [19, 20].

The same bands, refolded to the PBZ of the crystal, are shown in figure 3(b). At close magnification and inspection, a few localised states appear in the gap due to defects in the

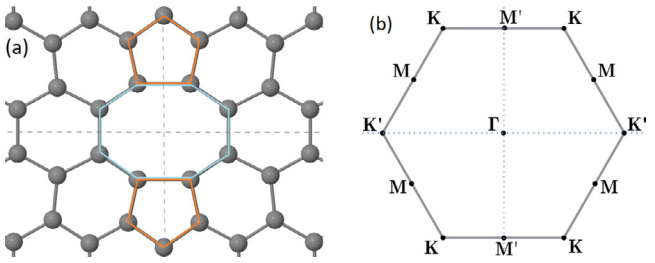

Figure 4. (a) Relaxed structure of the (585) divacancy in graphene. The dashed lines are the mirror planes of the defect. (b) PBZ of graphene, its symmetry modified by the (585) defect.

a-Si model [19]. Interestingly enough, despite its isotropic and non-periodic structure, and the incommensurability of its simulation cell with that of the crystal, the refolded bands of a-Si appear as a blurred version of the crystalline silicon (c-Si) bands, specially at low energies. Also, higher LDOS of a-Si can be appreciated in regions of c-Si band degeneracies. This similarity is independent of the size of the a-Si simulation cell employed. We attribute it to the similarity of the local structure in a-Si and c-Si in bond distances and angles [19].

Divacancy in graphene

Graphene is a material with unique electronic properties, but highly sensitive to structural disorder. The presence of defects leads to significant changes on its bands, specially around the Fermi level. Many types of defects have been studied by theorists, such as adatoms, vacancies or Stone–Wales defects, with the aim of predicting their properties and, potentially, using them to tailor the functionalities of graphene. Hence, unfolding their band stuctures will shed light on how they modify the original graphene bands.

We consider a (585) divacancy in a graphene monolayer, a defect that has been synthesised and characterised by Ugeda *et al* [21]. The (585) defect is formed by two adjacent C vacancies rearranged into two pentagons and one octagon, as shown in figure 4(a), with no dangling σ bonds. We modelled the divacancy in simulation cells of different sizes, from 7×7 to 14×14. Here we report the 11×11, 12×12 and 13×13 as representative.

The conventional bands of the supercell calculations within their SBZs, figure 5, reveal that the former six-fold symmetry of the Brillouin zone is broken, leading to inequivalent K and M points and two emerging mirror planes, figure 4(b), as happens in the atomic structure. The K and K' points no longer present a Dirac cone, although all of them present a band crossing of E_F at different points in their Brillouin zones: near K' for the 11×11 SC, around Γ for the 12×12 SC and between M' and K for the 13×13 SC. Besides this, it is hard to find similarities between them. To relate these overcrowded spectra with the band structure of graphene, we compute the refolded bands into the PBZ in the surroundings of K and K' points of graphene.

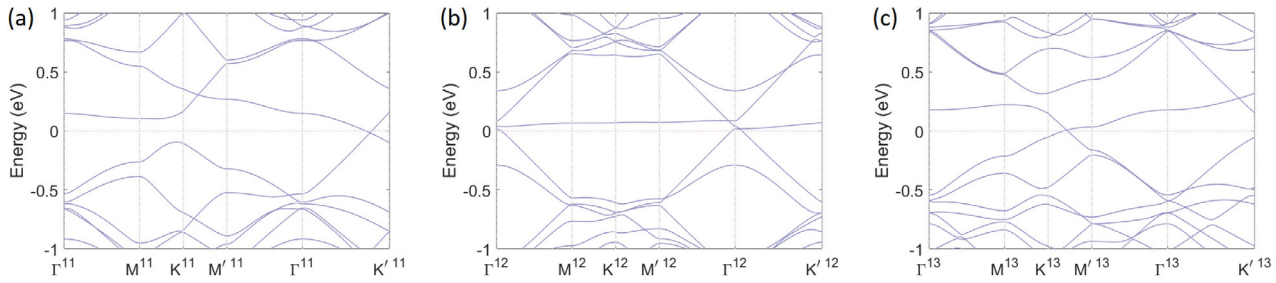

Figure 5. Conventional bands of a (585) divacancy in graphene modelled in (a) 11×11, (b) 12×12 and (c) 13×13 simulation cells, in their respective SBZs.

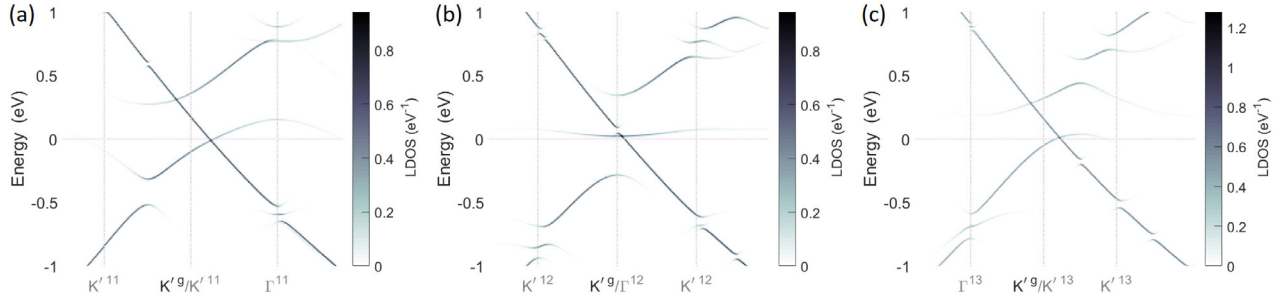

Figure 6. Bands around the Fermi level of a (585) divacancy in graphene, refolded into the PBZ, obtained from (a) 11×11, (b) 12×12 and (c) 13×13 simulation cells. K'^{g} denotes the K' point of the PBZ of graphene. K'^{n} indicates a K' point of the $(n \times n)$ SBZ.

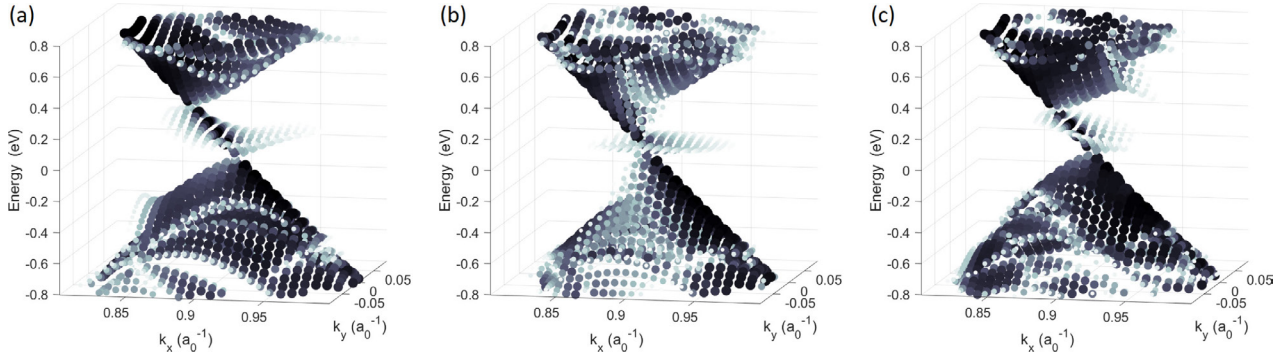

Figure 7. 2D bands of a (585) divacancy refolded into the PBZ, in the surroundings of the K' point, obtained from (a) 11×11, (b) 12×12 and (c) 13×13 simulation cells. The darkness times size of the dots is proportional to the LDOS, with weights smaller than a hundredth of the maximum neglected. The units for k are $1/a_0$, where a_0 is the lattice parameter.

Figures 6(a) and (c) show the 11×11 and 13×13 SC bands refolded into the PBZ. The Fermi level crossing is located around K' of graphene, which corresponds to a K' point in both SBZs. One of the bands conforming the former Dirac cone stays almost unaltered, while the other one is split, forming two cone tips shifted in the k_x direction and connected by a state. In the 2D bands plot of figures 7(a) and (c) this is seen with more clarity. The Fermi level decreases from its original value, being coincident with the tip of the lower cone.

In the case of the 12×12 SC, figure 6(b), we see a similar behaviour, with slight differences. One band of the cone remains almost unaltered, with a small gap of 0.04 eV opening at K'. The other one is split, with one of its fragments conforming a flat state at the Fermi level, leading to a single band crossing. In figure 7(b) this flat state and the cone tips can be appreciated. Here, the K' of graphene coincides with a Γ point of the 12×12 SBZ.

Despite the differences between the three sizes, a general trend is clearly identified after refolding into the PZB of graphene, which is not the case in the traditional bands description of figure 5. All cases present a splitting and a shift in k_x of the Dirac cone, as well as a single band between the two cone tips as the lowest unoccupied electronic state. The Fermi level is located at the tip of the lower cone. We remark that, in $3n \times 3n$ SCs, the K' of the PBZ corresponds to a Γ point in the SBZ, unlike in the $(3n+1) \times (3n+1)$ and $(3n+2) \times (3n+2)$ cases. This is consistent with the formal differences existing between both kinds of supercells [22]. Finally, the refolded bands obtained around K are inverted in k_y compared to the refolded bands around K' shown above.

Pressure in rotated graphene bilayers

Another path to modify the electronic behaviour of graphene is given by rotated graphene bilayers. These are defect-free

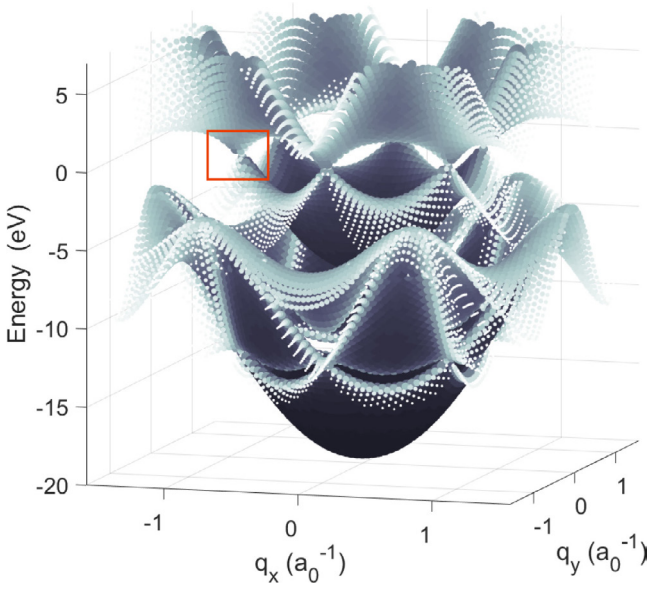

Figure 8. Fully unfolded bands of a graphene monolayer, up to the second Brillouin zone. The squared area marks a Dirac cone, region considered for further study in the bilayer case.

systems with a Moiré pattern, involving large periodicities. At small angles, the interaction between the two layers induces two saddle points in the band structure, along with two logarithmic van Hove singularities in the DOS. As the angle decreases, the singularities approach and, eventually, at the so called magic angles ($\theta = 1.1°$), they collapse into a single peak at the Fermi level [23]. The same effect has been recently reported to occur for larger angles, when external pressure is applied [24–27].

We study a bilayer rotated 5.08°, at equilibrium under increasing pressures up to 1.63 GPa. We employ a GGA exchange-correlation functional including Van der Waals interactions [28, 29]. As none of the monolayers lattice orientations has a prevalence over the other, refolding into the PBZ of one of them is not particularly informative. Therefore, we consider the fully unfolded bands as the adequate tool to analyze this system. We first show the fully unfolded bands of a graphene monolayer, figure 8, up to its second Brillouin zone, for comparison purposes. Two paraboloids with gaps opening along them and a six-fold symmetry and are clearly distinguished, and conform the dispersion relations of the σ and π orbitals. In the case of the bilayer, we will restrict the unfolding region to the surroundings of a K (and $K^{5.08°}$) point (red square).

In figure 9 we show the conventional band structures of the bilayer at the equilibrium distance, at a middle stage and under a pressure of 1.63 GPa, next to their corresponding DOS. The saddle points and van Hove singularities can be appreciated.

Figure 10 depicts the evolution of the fully unfolded spectra under increasing pressures. At equilibrium configuration, figure 10(a) shows a neat picture of the interaction between the cones of both monolayers, as well as the saddle

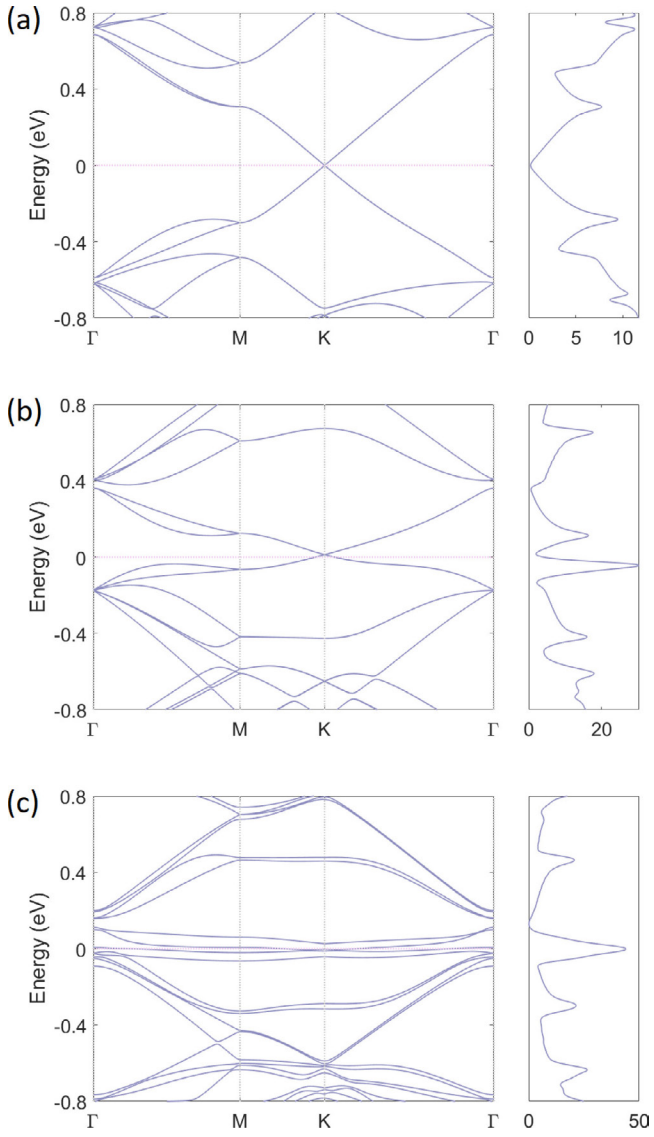

Figure 9. Conventional bands in the SBZ and DOS of a graphene bilayer rotated an angle of 5.08°, (a) at equilibrium geometry; (b) under a pressure of 0.70 GPa and (c) under 1.63 GPa.

point emerging in between. The relative maximum intensities of the LDOS are homogeneous in energies, and the states present high dispersion in energies. As pressure is applied, figures 10(b)–(e), the cones flatten and the saddle points move towards the Fermi level. We appreciate as well that the two pairs of bands immediately over and below the cones lower their energies and start to merge. Also, in figures 10(d) and (e), higher weights correspond to these merging bands, whereas the cone states around the Fermi level tend to be delocalized in many **q**s. In figure 10(f) the cones have collapsed into flat bands. We remark how their weight in this area of reciprocal space is small compared to that of the merging bands, despite the sharp peak on the DOS of figure 9(c). This is an indicator of delocalization in **q**, and is not unexpected, as these states are known to be well localized in the AA stacking region in real space [21, 24, 30].

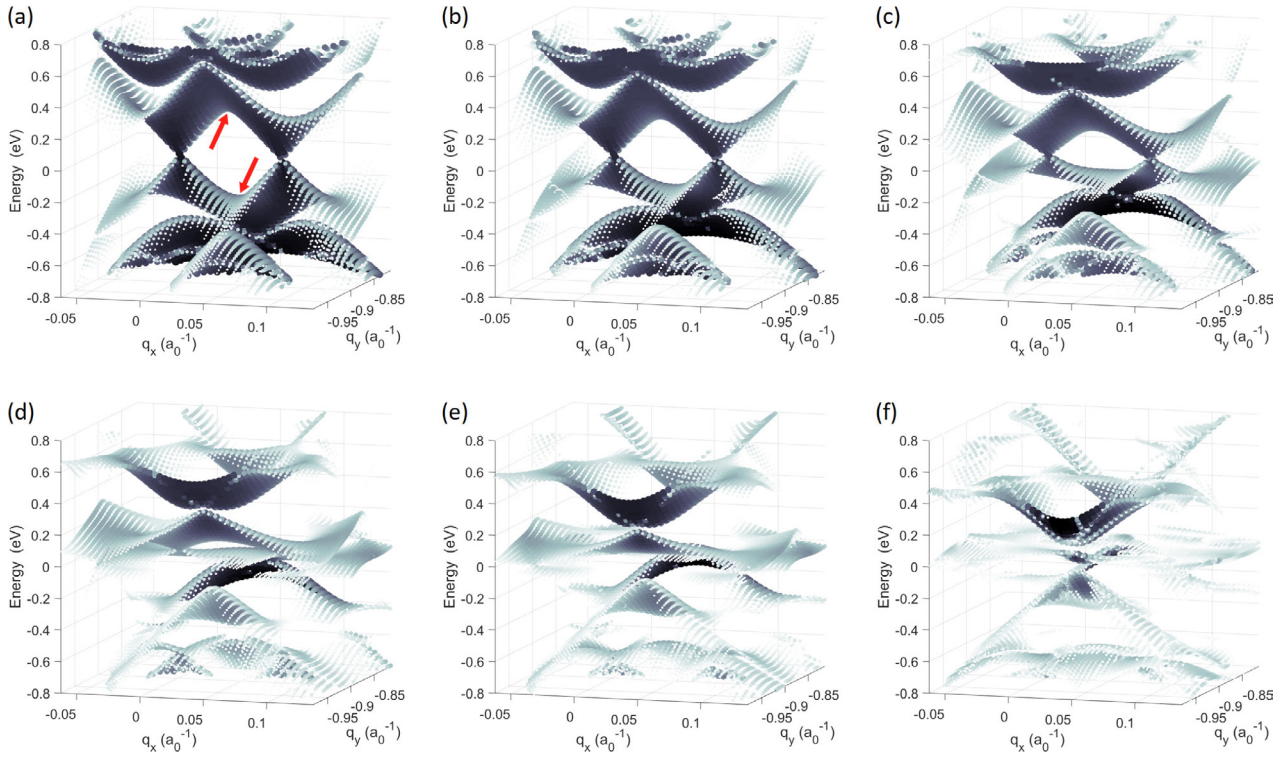

Figure 10. 2D fully unfolded bands of a graphene bilayer rotated 5.08°, in the surroundings of the first *K* points of the monolayers, at different pressures: (a) equilibrium distance. The arrows indicate the saddle points that originate the van Hove singularities; (b) 0.04 GPa; (c) 0.23 GPa; (d) 0.70 GPa; (e) 1.06 GPa and (f) 1.63 GPa.

Conclusions

We have presented a simple formulation of the band unfolding problem, a tool necessary to extract useful information from the band structure of large supercell calculations. The idea of a *full unfolding* that expands the bands not only to the primitive cell, but to the full reciprocal space, allows to treat this problem as a decomposition of the wave functions into its Fourier coefficients. A *refolding* recovers the conventional unfolded bands in the PBZ of the crystal. It is feasible for any eigenstate, regardless of the basis used. In the case of plane wave codes this implementation shall be almost immediate.

We have successfully applied our algorithm to obtain new characterizations of non-trivial physical systems. The fully unfolded bands provide a distribution of the states as a function of their energy and momenta, allowing a direct comparison with experimental photoemission spectra, as well as a way to determine a value of the effective mass of the system under study in a chosen direction of reciprocal space. Refolding into the primitive cell yields clear band spectra that allow comparison with the crystal bands, even identifying crystal-like patterns in an amorphous solid.

The outcomes of this work prove that the underlying state distribution in reciprocal space is much richer than what conventional band structures can evince, transcending the existence of any real or imposed periodicity.

Acknowledgments

We are grateful to B Battarai and D Drabold for sharing the coordinates of their a-Si model with us. JMS thanks Prof. P B Allen for introducing him into the unfolding problem. Funded by Spanish Government Grants FIS2015-64886-C5-5-P, MAT2017-83553-P and PGC2018-096955-B-C42.

ORCID iDs

Sara G Mayo https://orcid.org/0000-0001-9719-8022
Felix Yndurain https://orcid.org/0000-0003-0968-4050
Jose M Soler https://orcid.org/0000-0003-1046-7221

References

[1] Boykin T B and Klimeck G 2005 *Phys. Rev.* B **71** 115215
[2] Boykin T B, Kharche N, Klimeck G and Korkusinski M 2007 *J. Phys.: Condens. Matter* **19** 036203
[3] Boykin T B and Ajoy A 2018 *Physica* B **531** 130–8
[4] Dargam T G, Capaz R B and Koiller B 1997 *Phys. Rev.* B **56** 9625
[5] Lee C C, Yamada-Takamura Y and Ozaki T 2013 *J. Phys.: Condens. Matter* **25** 345501
[6] Chen M X and Weinert M 2018 *Phys. Rev.* B **98** 245421
[7] Ku W, Berlijn T and Lee C C 2010 *Phys. Rev. Lett.* **104** 216401

[8] Popescu V and Zunger A 2010 *Phys. Rev. Lett.* **104** 236403
[9] Popescu V and Zunger A 2012 *Phys. Rev.* B **85** 085201
[10] Allen P B, Berlijn T, Casavant D A and Soler J M 2013 *Phys. Rev.* B **87** 085322
[11] Huang H *et al* 2014 *New J. Phys.* **16** 033034
[12] Medeiros P V C, Stafström S and Björk J 2014 *Phys. Rev.* B **89** 041407
[13] Rubel O, Bokhanchuk A, Ahmed S J and Assmann E 2014 *Phys. Rev.* B **90** 115202
[14] Kosugi T, Nishi H, Kato Y and Matsushita Y 2017 *J. Phys. Soc. Japan* **86** 124717
[15] Himpsel F J and Eastman D 1979 *J. Vac. Sci. Technol.* **16** 1297
[16] Han C Q *et al* 2014 *Phys. Rev.* B **90** 085101
[17] Soler J M, Artacho E, Gale J D, Garcia A, Junquera J, Ordejon P and Sanchez-Portal D 2002 *J. Phys.: Condens. Matter* **14** 2745
[18] Perdew J P, Burke K and Ernzerhof M 1996 *Phys. Rev. Lett.* **77** 3865
[19] Igram D, Bhattarai B, Biswas P and Drabold D A 2018 *J. Non-Cryst. Solids* **492** 27–32
[20] Barber H D 1967 *Solid-State Electron.* **10** 1039
[21] Ugeda M M, Brihuega I, Hiebel F, Mallet P, Veuillen J Y, Gomez-Rodriguez J M and Yndurain F 2012 *Phys. Rev.* B **85** 121402
[22] García-Lastra J M 2010 *Phys. Rev.* B **82** 235418
[23] Cao Y, Fatemi V, Fang S, Watanabe K, Taniguchi T, Kaxiras E and Jarillo-Herrero P 2018 *Nature* **556** 43
[24] Yndurain F 2019 *Phys. Rev.* B **99** 045423
[25] Lopez-Bezanilla A 2019 *Phys. Rev. Mater.* **3** 054003
[26] Carr S, Fang S, Jarillo-Herrero P and Kaxiras E 2018 *Phys. Rev.* B **98** 085144
[27] Yankowitz M, Chen S, Polshyn H, Watanabe K, Taniguchi T, Graf D, Young A F and Dean C R 2019 *Science* **363** 1059
[28] Berland K and Hyldgaard P 2014 *Phys. Rev.* B **89** 035412
[29] Román-Pérez G and Soler J M 2009 *Phys. Rev. Lett.* **103** 096102
[30] Trambly de Laissardire G, Mayou D and Magaud L 2012 *Phys. Rev.* B **86** 125413